





Realization of in Situ Fiber-Core Temperature Measurement in a Kilowatt-Level Fiber Laser Oscillator: Design and Optimization of the Method Based on OFDR

Zhaokai Lou , Kai Han , Baolai Yang , Hanwei Zhang , Xiaoming Xi, Xiaolin Wang, Xiaojun Xu, and Zejin Liu

Abstract—High-power fiber lasers have been widely used in various industrial manufacturing and military defense applications. During the development of fiber lasers in the past decades, the thermal effect has always been one of the biggest obstacles. It is crucial to study the temperature characteristics and overcome the thermal restrictions for a better output performance. With the systematic design and optimization in this article, optical frequency domain reflectometry (OFDR) can achieve in situ distributed temperature measurement of the fiber core in high-power fiber lasers. This allows a better study of the temperature characteristics and thermal effects. The fiber-core distributed temperature of a kilowatt-level fiber oscillator is first demonstrated based on this method here. The splicing point between the high reflectivity fiber Bragg grating (HR-FBG) and gain fiber withstands the highest temperature, reaching 101.6 °C at a 1.47 kW output. In addition, the temperature of the gain fiber gradually decreases from 92 °C to 30 °C along the pumping direction. The internal temperatures of the combiner and HR-FBG are also measured to evaluate their performances in the high-power regime. The temperature distributions in the experiment agree well with the theoretical simulation.

Index Terms—Fiber core temperature, fiber laser, OFDR, temperature characteristics.

I. INTRODUCTION

HIGH power fiber lasers have been widely utilized in many industrial, defense, and scientific applications due to their advantages of high conversion efficiency, good beam quality, and large surface-to-volume ratio, which lead to excellent heat dissipation capability [1]–[3]. In the last few decades, the output power of nearly single-mode fiber laser amplifiers and oscillators

Manuscript received September 16, 2020; revised November 10, 2020; accepted December 9, 2020. Date of publication January 1, 2021; date of current version April 16, 2021. This work was supported in part by the National Natural Science Foundation of China (NSFC) under Grant 61605245. (Zhaokai Lou and Kai Han contributed equally to this work.) (Corresponding author: Kai Han.)

The authors are with the College of Advanced Interdisciplinary Studies, State Key Laboratory of Pulsed Power Laser Technology and Hunan Provincial Key Laboratory of High Energy Laser Technology, National University of Defense Technology, Changsha, Hunan 410073, China (e-mail: louzhaokai11@nudt.edu.cn; hankai0071@nudt.edu.cn; yangbaolai1989@163.com; zhanghanwei100@163.com; exixiaoming@163.com; chinawxllin@163.com; xu_xiaojun@126.com; zejinliu@nudt.edu.cn).

Color versions of one or more figures in this article are available at <https://doi.org/10.1109/JLT.2020.3048747>.

Digital Object Identifier 10.1109/JLT.2020.3048747

has experienced a dramatic increase, reaching 20 kW and 5 kW, respectively [4]–[6]. With the improvement of the output power, the thermal effect has become one of the biggest limitations in the development of fiber lasers [1]–[3]. The temperature rise and thermal accumulation along the fiber core may lead to destructive self-pulsing [7], thermal lensing [8], [9], fiber fuse phenomenon [10], and transverse mode instability (TMI) [9], [11]. Recent years have witnessed growing academic interest in the temperature characteristics and thermal effects in the high power regime. Many mature theoretical models have been built for thermal analysis of fiber lasers [12]–[14], while experimental studies measuring the real fiber-core temperature are still insufficient. Therefore, there is an urgent need to measure the temperature of the fiber core in fiber lasers to provide a better study of the thermal effects and allow a greater possibility for a breakthrough.

To date, the most common methods for temperature measurement of fiber lasers include the use of thermal imagers, thermocouples, or thermal resistance. However, these methods can only measure the temperature from the outside instead of inside the core. In high-power fiber laser regimes, the temperature of the fiber core could be significantly different from the temperature of the fiber coatings [13]. Carving fiber Bragg gratings (FBGs) into the gain fiber is regarded as an implementable method for fiber-core temperature measurement [15], [16]. Nevertheless, it can only provide limited spot information and probably influences the performance of the carved gain fibers in the high power regime. Recently, coherent reflectometry has already been used to achieve in situ distributed fiber-core temperature measurement [17], [18]. Moreover, optical frequency domain reflectometry (OFDR) is one of the most powerful and befitting tools due to its high spatial resolution, temperature resolution, and precision [19]. The response speed of OFDR systems (\sim Hz level) is also sufficient for in situ measurement of fiber lasers.

Generally, a high-power fiber laser can be achieved based on two structures: the master oscillator power amplification (MOPA) structure and the monolithic fiber laser oscillator structure. Compared with the MOPA structure, monolithic fiber laser oscillators enjoy the advantages of a simpler structure, fewer components, and easier operation [20]. However, fiber-core

temperature measurement in a fiber laser oscillator by OFDR is more difficult than that in the MOPA structure because the cavity in the oscillator causes stronger backward lasers, which could reduce the signal-to-noise ratio in the measurement system. The higher the output power is, the stronger the backward laser. In 2017, Franz B. et al. measured the temperature of the gain fiber core in kilowatt-level fiber amplifiers by OFDR [18]. However, detailed measurement methods with OFDR have not been given. The thermal effects of fiber laser oscillators and fiber laser amplifiers are different. To date, the fiber-core temperature in high-power multimode fiber laser oscillators has not been reported. Additionally, a systemic summary is required to shed light on how to apply the OFDR technique in the field of optical fiber sensing to the field of high-power fiber lasers.

Recently, our group has mastered and achieved a fiber-core temperature measurement technique in the high power regime. This technique has been applied in the study of nonlinear effect suppression by temperature modulation [21]. The fiber-core temperature in hundred-watt-level single-mode fiber laser oscillators has also been previously obtained [22]. In fiber laser oscillators, breakthroughs from hundred-watt-level single-mode fibers to kilowatt-level multimode fibers are difficult to realize because of the strong backward laser and low signal-to-noise (SNR) ratio. In this paper, we analyzed the obstacles to and demonstrated solutions for the realization of fiber-core temperature measurement in a high power regime. By systematic design and optimization, the fiber-core temperature in kilowatt-level multimode fiber laser oscillators was demonstrated. The experimental results agreed well with the simulation results of the theoretical model, which verified the feasibility and validity of the method. To the best of our knowledge, this is the first fiber-core temperature measurement in kilowatt-level laser oscillators and the first systemic summary of the cross application of the OFDR technique between the field of optical fiber sensing and the field of high-power fiber lasers.

II. METHOD DESIGN AND OPTIMIZATION

A. Theory of the Measurement Method

The OFDR technique was put forward in the field of optical fiber sensing by Eickhoff as early as 1981 [23]. The OFDR system we used in our experiment is a commercial and powerful system called ODiSI-B, which was developed by LUNA Innovation. In our operation mode, this ODiSI-B system enables temperature measurements at a spatial resolution of up to 2.6 mm along the sensing fiber and a temperature resolution of 0.1 °C. The scan wavelength range is from 1523.6 nm to 1569.6 nm, and the measurement frequency of the in situ system is 4.17 Hz. The algorithm applied for temperature change calculations and further comprehensive information about the Luna system are presented elsewhere [24]–[27]. The fundamental component of the OFDR system is an interferometer, as shown in Fig. 1. The linear sweep light source in OFDR is divided into two parts by Coupler 1. One part of the linear sweep light passes through the circulator and fiber under test, which produces backward Rayleigh scattering as the signal light. Then, the backward signal light is transmitted into a photoelectric detector through the circulator and Coupler 2. The other part of the linear sweep light

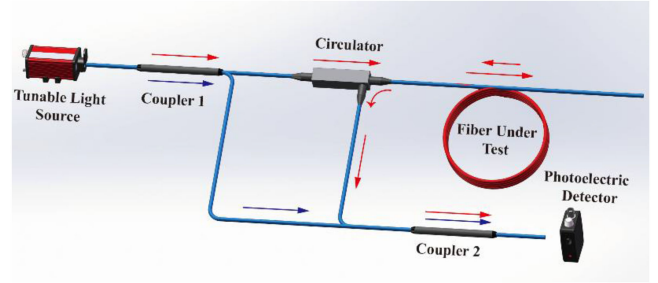


Fig. 1. Fundamental structure of the OFDR system.

is directly transmitted into the photoelectric detector through Coupler 2 as reference light.

Here, we assume that the optical field of the light source is $E(t)$, which can be expressed as (1).

$$E(t) = E_0 \exp \{j [2\pi(f_0 + \gamma t)t]\} \quad (1)$$

where E_0 denotes the amplitude of the reference light and f_0 represents the original frequency of the linear sweep light. γ is the tuning speed of the tunable linear sweep light, and t is time. For the optical field of backward signal light, we take the optical information reflected from a certain point in the fiber under test as an example. The time delay between the reference light and the backward signal light from this point is assumed to be τ . Then, the optical field of backward signal light from a certain point in the fiber under test can be expressed as (2).

$$E_R(t) = \sqrt{R}E(t - \tau) = \sqrt{R}E_0 \cdot \exp \{j [2\pi(f_0 + \gamma t - \gamma\tau)t] + C\} \quad (2)$$

Here, R denotes the reflectivity of backward Rayleigh scattering in the fiber under test, and C is the constant term in the optical field. Finally, the photoelectric detector detects the mixed signals of the backward signal light and the reference light. Therefore, the photocurrent in the detector can be expressed as (3).

$$i(t) = |[E(t) + E_R(t)]|^2 = |E(t)|^2 + |E_R(t)|^2 + 2\sqrt{R}E_0^2 \cos(4\pi\gamma\tau t) \quad (3)$$

In (3), the first two items represent the direct currents, which contain no reflected information about the fiber under test. The last item is the alternating current, whose frequency corresponds to the location information and intensity corresponds to the backward Rayleigh scattering intensity. By analyzing the Fourier transform of (3), the spectrum information of backward Rayleigh scattering light can be obtained as shown in (4). Here, we focus on the spectral shift of the backward Rayleigh scattering light.

$$S(f) = \left| \int_{-\infty}^{\infty} i(t)e^{j2\pi ft} dt \right|^2 \quad (4)$$

Meanwhile, the fiber under test can be regarded as a weakly random periodic grating that is continuously distributed. The temperature variation in the fiber core causes a spectral shift of the backward Rayleigh scattering light. Therefore, we can transform the spectral information into temperature information based on the relationship between the temperature variation and spectral shift. The relationship between the spectral shift and

temperature variation in the absence of strain changes is shown in (5).

$$\frac{\Delta\lambda}{\lambda} = \frac{\Delta\nu}{\nu} = K_T \Delta T \quad (5)$$

where λ and ν are the mean optical wavelength and frequency, ΔT is the temperature variation, and K_T is the sensitivity response to temperature variation.

According to (5), we can analyze the temperature variation in the fiber core in a free state once we obtain the spectral shift of the signal light in the absence of a strain change. However, measuring the absolute temperature of the fiber core under laser operation is challenging. Many obstacles need to be solved to achieve this goal. First, the data measured by OFDR are the temperature variation rather than the real temperature. Additionally, the sensitivity response to temperature variation varies in different kinds of fibers. To obtain the real temperature, the sensitivity response to temperature variation needs to be confirmed, and the temperature needs to be calibrated. Second, the gain fiber coiled on the plate would undergo a strain change, which would affect the temperature measurement. Finally, the loss of the signal light from the OFDR system cannot be neglected because of the complex structure and various components in the fiber laser system. Additionally, the noise is strong in the high-power laser system because of the strong backward laser. Therefore, the signal-to-noise (SNR) ratio is too low to achieve fiber-core temperature measurement. In the next parts, we present our analysis of and solutions to these obstacles.

B. Calibration of the Fiber under Test

According to (5), after analyzing the spectral shift measured by OFDR, the results we can obtain are the variations in fiber-core temperature instead of the absolute values. Moreover, the values for K_T are somewhat dependent on the doping type and concentration in the core of the fiber. Therefore, calibrations are needed to confirm the value of K_T and to transform the relative value to the absolute temperature value. For the calibration process, the reflected spectrum of the fiber in the system at room temperature was first measured as the reference profile. Then, the fiber under test was put into an incubator at a certain steady temperature. Thermoelectric couples were applied to measure the incubator temperature, which was regarded as the real temperature after the fiber under test reached thermal equilibrium. Then, the reflected spectrum was measured by OFDR again. After the cross-correlation of these two reflected spectra, we obtained the spectral shift at this incubator temperature. Detailed figures and descriptions of wavelength spectra and cross-correlation can be found in [28]–[31]. By repeating this process at other incubator temperatures, the relationship between the real temperatures and spectral shifts measured by OFDR could be obtained.

Here, we performed the calibration for a ytterbium-doped cladding step-index multimode fiber with a core diameter of 20 μm and a cladding diameter of 400 μm in our experiment. During the calibration, the incubator temperature was adjusted to 5 $^\circ\text{C}$, 10 $^\circ\text{C}$, 15 $^\circ\text{C}$, 20 $^\circ\text{C}$, 23 $^\circ\text{C}$, 30 $^\circ\text{C}$, 40 $^\circ\text{C}$, 50 $^\circ\text{C}$, 60 $^\circ\text{C}$, 70 $^\circ\text{C}$, and 80 $^\circ\text{C}$. The measured spectral shifts $\Delta\lambda/\lambda$ are -9.92×10^{-5} , -7.34×10^{-5} , -4.76×10^{-5} , -2.36×10^{-5} , $-7.17 \times$

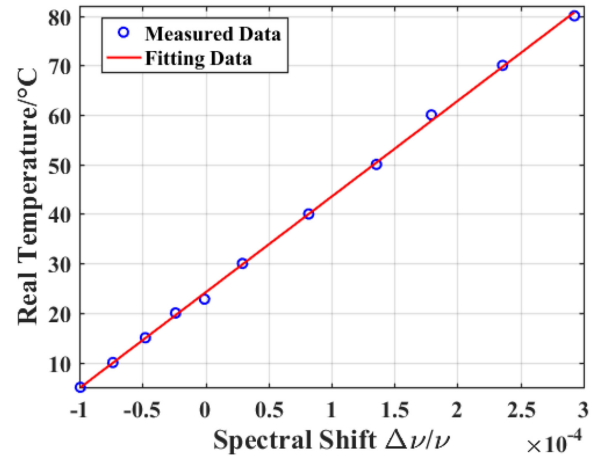


Fig. 2. Relationship between the real temperature and spectral shift measured by OFDR.

10^{-7} , 2.94×10^{-5} , 8.20×10^{-5} , 1.36×10^{-4} , 1.79×10^{-4} , 2.36×10^{-4} , and 2.93×10^{-4} , respectively. From these two series of data, the linear fitting curve and the linear fitting equation can be obtained as shown in Fig. 2 and (6). In 6, T represents the real temperature. With the calibration equation, the relative temperature can be transformed to the real temperature for the fiber under test.

$$T = 1.93 \times 10^5 \frac{\Delta\lambda}{\lambda} + 24.13 \quad (6)$$

C. Decoupling of Temperature and Strain

According to (5), a linear relationship between the temperature variation and spectral shift is demonstrated. It is worth noting that if the fiber under test undergoes a change in strain, then the reflected spectrum at that location will experience a shift in optical frequency. Therefore, the spectral shift can usually be related to both temperature and strain changes. (5) should be modified by a strain term to (7).

$$\frac{\Delta\lambda}{\lambda} = \frac{\Delta\nu}{\nu} = K_T \Delta T + K_\varepsilon \Delta\varepsilon \quad (7)$$

where $\Delta\varepsilon$ is the variation in strain in the fiber, and K_ε is the sensitivity response to strain variation. Therefore, after we first measure the Rayleigh scattering signature as the reference profile in an ambient state, the fiber under test must remain stable without any movement, stress, or strain for the remaining steps of fiber-core temperature measurement. Especially with the air-cooling or water-cooling machines used for the high-power laser regime, the optical platform easily vibrates, which causes strain variation and affects the temperature measurement. In our experiment, water-cooling machines with low vibration and antivibration optical platforms were applied for fiber-core temperature measurement in the high-power regime. The fiber under test fit the platform perfectly without hanging in the air in case of vibration.

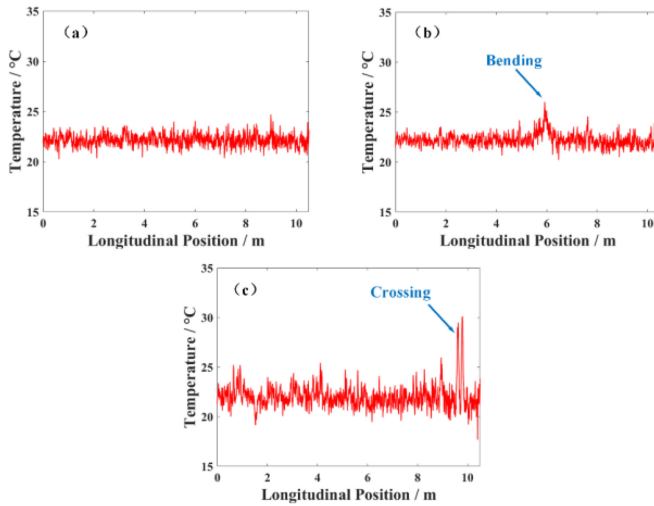


Fig. 3. Comparison of the gain fiber core temperatures in the fiber laser system (a) without residual strain, (b) with bending, and (c) with crossing.

In addition, we not only prevented strain variation after we first measured the Rayleigh scattering signature but also tried to eliminate the residual strain while we coiled the fiber on the platform. According to our experimental experience, there would be residual strain along the fiber under test if some points on the fiber are even slightly twined, spun, bent, or crossed. These corresponding points with residual strain would cause temperature anomalous points. The higher the output power is, the more obvious the temperature anomalous points.

Here, we compared the difference in the fiber core temperatures in gain fibers with or without residual strain, as shown in Fig. 3. Fig. 3(a) shows the gain fiber core temperature distribution in a fiber laser amplifier without residual strain, while Fig. 3(b) and (c) present the results for the gain fiber with localized bending and crossing, respectively. In Fig. 3(a), the gain fiber was coiled in the water-plate in a regular diameter (from 38 cm to 40 cm). In Fig. 3(b), an improper bending was introduced to simulate the localized residual strain at 5.9 meters away from the start of the gain fiber. At this localized position, the diameters of the bending was mutated to 7 cm, while the fiber at other positions remained normal bending diameter. Therefore a significant protrusion is observed along the temperature distribution at this localized position while the other places remain normal. In Fig. 3(c), a localized crossing happened at approximately 9.7 meters away from the start of the gain fiber. At this localized position, two different parts of the gain fiber crossed each other which should have been separated in different tracks. Therefore two obvious peaks appeared along the temperature distribution during laser operation. These two peaks are related to the positions of two intersecting points (9.63-meter and 9.80-meter position) because of crossing. These protrusions and peaks are temperature anomalous points that should be eliminated. Therefore, during the fiber coiling process, OFDR is also needed to help us find, locate, and eliminate these temperature anomalous points with a low power state in the system. After ensuring that the fiber under test is coiled

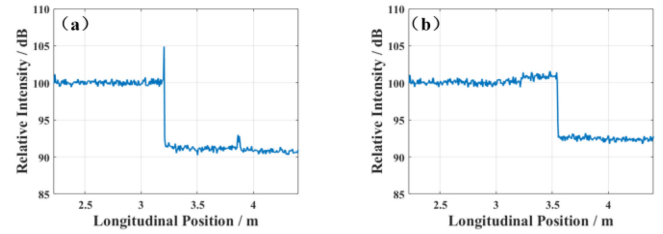


Fig. 4. Comparison of splicing losses between two kinds of fibers: (a) direct splicing and (b) with an MFA (mode field adapter).

without anomalous points and residual strain in a low power state, the fiber can be fixed with special glue on the water-cooling platform.

D. Loss Reduction of Signal Light

The signal-to-noise ratio (SNR) is the key factor in determining whether the fiber-core temperature can be measured by OFDR. To improve the SNR, the first step is to reduce the signal light loss. For the fiber-core temperature measurement system, three main aspects can be optimized to achieve loss reduction of the signal light, which concentrate on a mode field adapter (MFA), splicing points, and the coiling diameter.

1) *Application of an MFA:* In the field of distributed optical fiber sensing, common single-mode communication fibers are generally used, with a core diameter of approximately $10\ \mu\text{m}$. Meanwhile, in the field of high-power fiber lasers, multimode gain fibers are usually used, with a core diameter of approximately $20\ \mu\text{m}$ or greater. Therefore, if we want to apply optical fiber sensing technology to the high-power field, splicing points between these two kinds of fibers and the resulting loss will be inevitable. The use of an MFA to splice these two kinds of fibers causes less signal light loss than direct splicing, thereby effectively improving the SNR. We compared the loss differences between these two cases, as shown in Fig. 4. Here, the OFDR system is used to measure the relative intensity of the backward Rayleigh scattering over the length of the fiber, which reflects the signal light loss. In this comparison, we optimized the splicing parameters and improved the splicing many times; however, a significant drop in the relative intensity of the backward Rayleigh scattering can still be seen in Fig. 4(a) of approximately 9.42 dB. A reflection peak can also be observed right at the splicing point between the two kinds of fibers, which will result in poor temperature measurement at this point. With the application of the MFA, elimination of the reflection peak is recorded in Fig. 4(b). Moreover, the intensity loss of the backward Rayleigh scattering decreases by approximately 2.2 dB. Therefore, an MFA is an indispensable device for applying OFDR technology to the high-power field.

2) *Influence of Splicing Points:* The quality of the splicing points has always been one of the key issues in the field of high-power fiber lasers. In addition to the mismatched fiber splice mentioned in the above section, the quality of other splicing points will also have an important impact on the loss of the OFDR signal light, especially between passive fibers and

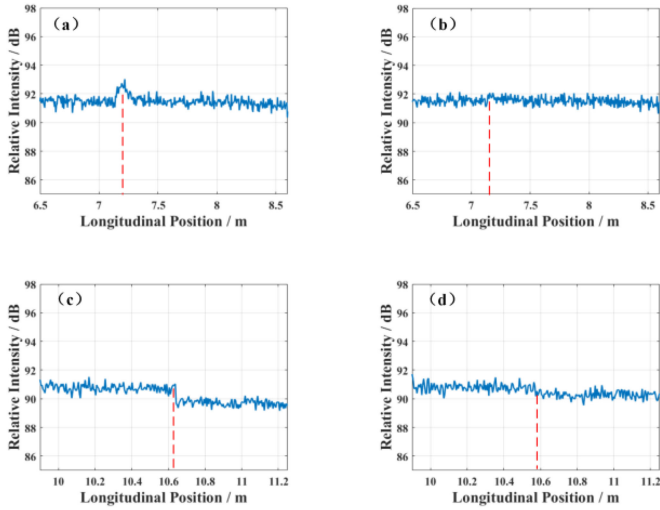


Fig. 5. Backward Rayleigh scattering relative intensity distribution along the fiber. (a) and (b) present the splicing loss between the HR-FBG and gain fiber before and after splicing optimization; (c) and (d) present the splicing loss between the gain fiber and OC FBG before and after splicing optimization.

gain fibers. Although the diameters of passive fibers and gain fibers match, they have other differences in core shape and doped material, which will cause laser loss after splicing. These losses may be negligible for the main laser and pump laser in the high power regime, but they have non-negligible effects on the signal light of fiber-core temperature measurement.

In the experiment, we repeatedly studied the splicing parameters of passive fibers and gain fibers. After many improvements, we optimized all the splicing losses within an acceptable range for fiber-core temperature measurement. Here, we show the backward Rayleigh scattering relative intensity distribution along the fiber with splicing points before and after splicing optimization in Fig. 5, where the fibers share the same core diameters of $20\ \mu\text{m}$ and cladding diameters of $400\ \mu\text{m}$. The positions marked by red lines correspond to the splicing point locations. From Fig. 5(a) and 5(b), we can see the changes at the splicing point between the fiber pigtail of the high reflectivity (HR) fiber Bragg grating (FBG) (left side of the red line) and the gain fiber (right side of the red line) before and after splicing optimization. Before splicing optimization, a significant backward Rayleigh scattering reflection peak at the splicing point can be observed, which would affect the temperature measurement at that location. By splicing optimization, the reflection peak can be eliminated, as shown in Fig. 5(b). Fig. 5(c) and 5(d) shows the changes at the splicing point between the gain fiber (left side of the red line) and the fiber pigtail of the output coupler (OC) FBG (right side of the red line) before and after splicing optimization. After splicing optimization, a reduction of 0.64 dB can be achieved for the loss at the splicing point. Here, due to the shortened fibers after splicing optimizations, the positions of the splicing points in Fig. 5(b) and 5(d) moved compared to the positions in Fig. 5(a) and 5(c).

3) *Optimization of the Coiling Radius:* The coiling state of fibers under test on the platform will cause bending loss of the

signal light emitted by the OFDR system, thereby affecting the SNR. According to the model with the bending loss formula presented by Marcuse [32]–[34], the 1550 nm signal light is more sensitive to bending loss than the 1080 nm laser. Therefore, the bending loss of the signal light cannot be ignored when we want to improve the SNR of the fiber-core temperature measurement system. In this section, we applied a 12.5 m ytterbium-doped fiber (YDF) with a core diameter of $20\ \mu\text{m}$ and a cladding diameter of $400\ \mu\text{m}$ in the fiber-core measurement system. The SNR in this system is determined by comparing the difference between the backward Rayleigh scattering intensity and the background noise. While continuously changing the coiling radius of the YDF, we found that the smaller the coiling radius is, the lower the SNR of the system. Without changing other factors in the system, the SNR at coiling radii of 22 cm \sim 25 cm, 17 cm \sim 20 cm, and 12 cm \sim 15 cm is increased by approximately 0.84 dB, 0.71 dB, and 0.65 dB respectively, compared to that at coiling radii of 7 cm \sim 10 cm. The coiling radius has a great effect on the loss of the signal light in the system. Furthermore, the increase in the numerical aperture (NA) due to the higher core temperature during laser operation could mitigate this loss. According to the thermo-optical coefficients [35] and temperature changes in 1.4 kilowatt laser system, the NA would increase by 4.9% after thermal equilibrium. According to the model mentioned above, when the bend radius is ~ 7 cm, which is a common small coiling radius for high beam quality in laser system, the bending loss would decrease by ~ 0.028 dB/m with the NA increasing by 4.9%. This is not a significant influence but still can make the SNR a little better, which is useful for the fiber-core temperature measurement in small coiling radius. In high power laser regime, small radius is useful for high beam quality of laser output. According to our experimental experience, the coiling radius is better not be lower than 7 cm, which would cause too large loss to achieve the fiber-core temperature measurement. The determination of the coiling radius is affected by many factors in the high power and high beam quality regime. Even so, if we want to improve the SNR for the measurement system, enlarging the coiling diameter appropriately is still an efficient method.

E. Noise Suppression in the System

Suppression of the noise is another key method to improve the signal-to-noise ratio. In the high-power fiber laser regime, most of the noise is caused by the backward light of the main laser and pump laser, which is one of the difficulties in applying fiber sensing technology. Moreover, due to the resonant cavity, the backward laser intensity in oscillators would be much stronger than that in amplifiers. The higher the output power is, the stronger the noise intensity. Here, we provide two methods to suppress the noise in high-power fiber lasers: one is to optimize the cutting angle, and the other is to apply wavelength division multiplexers (WDMs).

1) *Optimization of the Cleaving Angle:* The feedback intensity at the end of the fiber under test needs to be reduced to decrease the influence of noise, such as backward light from the main laser and pump laser. The most effective method is cleaving the end of the fiber at an optimum angle. In this section, we tested

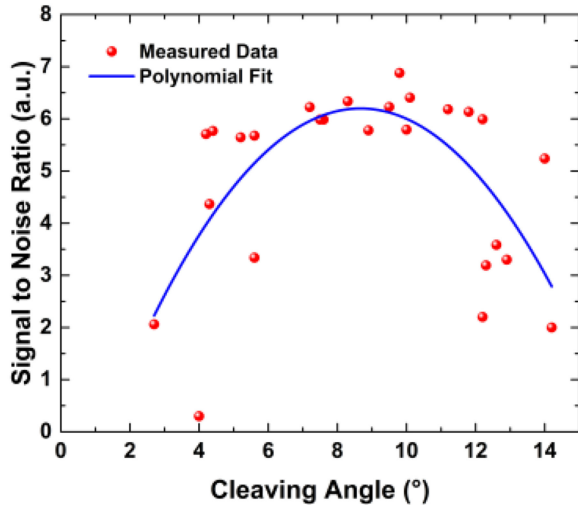


Fig. 6. Relationship between the relative SNR and cleaving angle at the end of the fiber.

the multimode fibers with core diameters of $20\ \mu\text{m}$ and cladding diameters of $400\ \mu\text{m}$. Different cleaving angles were obtained by a CT-106 optical fiber cleaver developed by Fujikura Company. Here we use the splicer observation system in a 100 P+ fusion splicer produced by Fujikura to measure the cleaving angle of the fiber. When other factors remain the same, the relationship between the relative SNR and cleaving angle at the end of the fiber is shown in Fig. 6.

As we can see, while the cleaving angles are under about 9° , the relative SNR shows an upward trend with the increase of the cleaving angle. That is because the feedback intensity of noise decreases monotonically with increasing cleaving angles at this angle range.

Besides, we think the cleaving quality could also affect the SNR of the system. In our experiment, we have studied the relationship between the cleaving quality and cleaving angle with a 20-fold microscope. Here are four representative optical images of fiber cross-section under different cutting angles in Fig. 7. While the cleaving angles are under approximately 9° , the cross-section of fibers are relatively smooth and flat, as shown in Fig. 7(a) and Fig. 7(b). While the cleaving angles exceed approximately 9° , there would be some jagged tracks on the surface of the fiber cross-section, which are shown in Fig. 7(c) and Fig. 7(d). These scratches continue to extend towards the fiber core from the edge of fiber cladding with the increase of cleaving angles and thereby increasing the feedback intensity of noise. Therefore the poor cleaving quality would also reduce the SNR while the cleaving angles are too large. During the experiments, the cleaving quality is not always stable. The cleaving qualities can be different even under the same cleaving angle. Therefore the SNR data shows a high level of dispersion in Fig. 6. But we can still get the general tendency here.

In conclusion, when the cleaving angles are under approximately 9° , the main factor for SNR is the cleaving angle. And the bigger the cleaving angle is, the lower the feedback intensity of noise. When the cleaving angles exceed approximately 9° ,

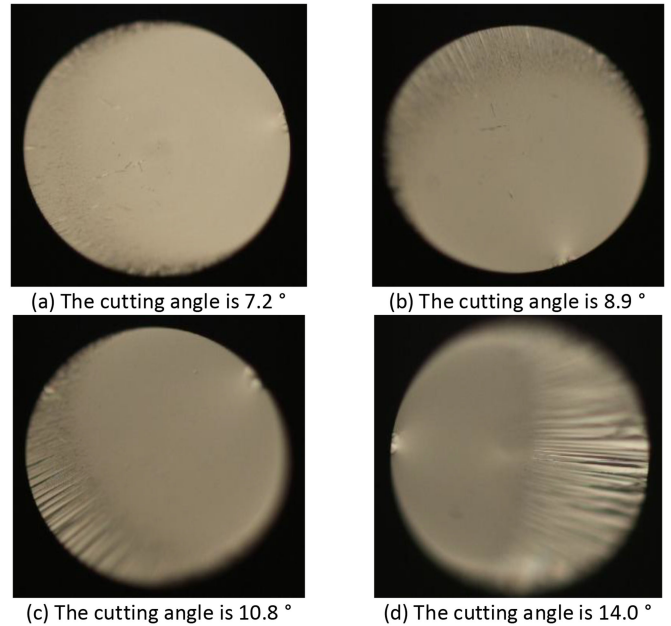


Fig. 7. Optical images of fiber cross-sections for different cutting angles.

the cleaving quality becomes an important factor for SNR. Furthermore, the cleaving quality becomes poorer with the increase of angle, and hence reduces the SNR. Therefore the SNR would show an upward trend first and then experience a downward trend with the increase of cleaving angle. The optimal angle interval is approximately 8° to 10° for fiber-core temperature measurement, which can most likely decrease the feedback intensity and thereby obtaining a higher SNR.

2) *Application of WDMs*: For a hundred-watt or even kilowatt laser regime, the intensity of backward light caused by the main laser and pump light can far exceed the power of the OFDR signal light. Therefore, WDMs are necessary to isolate backward light to ensure the safety of the measurement system and a high SNR. In our experiment, the wavelength of the signal light is $1550\ \text{nm}$, and the wavelength of the main laser is $1080\ \text{nm}$. The linearly swept signal light ($1550\ \text{nm}$) can be launched into the high-power laser system via the $1550\ \text{nm}$ port of a high-power $1080/1550\ \text{nm}$ WDM. Therefore, the use of $1.55\ \mu\text{m}$ beams from the OFDR system enables us to obtain spatially resolved Rayleigh frequency shifts of the YDF laser without disturbing the gain medium. It is worth noting that the backward light of kilowatt-level fiber laser systems is so strong that we may need three cascaded WDMs to isolate the main laser. The experimental setup of cascaded WDMs is shown in the next experimental section.

III. EXPERIMENTAL SETUP

The experimental setup to measure the fiber-core temperature in a kilowatt-level fiber laser oscillator is depicted in Fig. 8. Here, six groups of $976\ \text{nm}$ laser diodes (LDs) are used as pump sources, which are high-power wavelength stabilized. In each group, six LDs are spliced to a 7×1 combiner, and each LD module provides a maximum pump power of $\sim 60\ \text{W}$. Then,

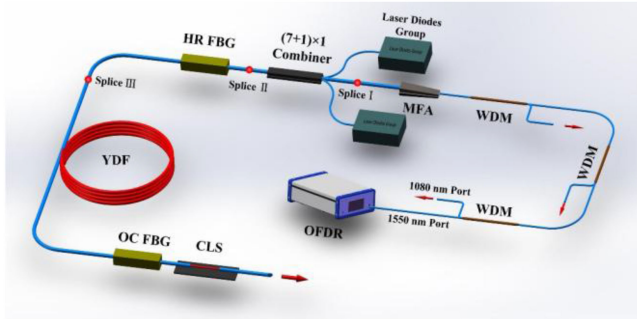


Fig. 8. Experimental setup to measure the fiber-core temperature of a kilowatt-level fiber laser oscillator.

these six groups of LDs ($6 \times 6 \times 60$ W) are inserted into the system via a $(7 + 1) \times 1$ high-power combiner. Compared to the 7×1 combiner in the branch, the $(7 + 1) \times 1$ high-power combiner in the trunk can withstand a higher power pump laser and has a signal port in the fiber bundle, which is for signal light propagation into the fiber core of the fiber laser. The pump ports of these two kinds of combiners are multimode fibers with core/cladding diameters of $220/242 \mu\text{m}$, and the unoccupied ports are angle cleaved to avoid facet reflection. The $(7 + 1) \times 1$ high-power combiner combines the pump light into the inner cladding of the output fiber with a diameter of $400 \mu\text{m}$ and then into the cavity. The resonant cavity of the fiber oscillator is formed by a pair of fiber Bragg gratings (FBGs) centered at 1080 nm with a high reflectivity of 99.7% and a low reflectivity of 10.7% . The gain fiber, a ytterbium-doped cladding step-index fiber (YDF), has a core diameter of $20 \mu\text{m}$ and a cladding diameter of $400 \mu\text{m}$. The peak cladding absorption efficiency of the YDF at 976 nm is 1.2 dB/m . To ensure adequate absorption of the pump light, a $\sim 12.5 \text{ m}$ long YDF is adopted as the gain medium for the laser. After the OC FBG, a delivery fiber with cladding light strippers (CLS) is utilized to fully dump residual pumping light that propagates in the inner cladding. All of the components mentioned above, including LDs, combiners, FBGs, and CLS, are placed on a water-cooled heat sink to carry away the accumulated heat, into which 20°C flowing water is injected.

The linearly swept signal light (1550 nm) emitted by the OFDR system is launched into the resonant cavity, successively passing through three cascaded high-power $1080 \text{ nm}/1550 \text{ nm}$ WDMs, an MFA ($10/125 \mu\text{m}$ to $20/400 \mu\text{m}$), and the signal port of the $(7 + 1) \times 1$ high-power combiner. Three cascaded WDMs are applied to improve the SNR and ensure the safety of the OFDR system. Both transmission and reception of the 1550 nm signal light occur via the 1550-nm ports of the high-power WDMs. Moreover, the backward noise light from the cavity is nearly eliminated through the three 1080 nm ports of the WDMs. The core/cladding diameters of the fiber tail in the OFDR system and WDMs are approximately $10/125 \mu\text{m}$, while the signal port of the $(7 + 1) \times 1$ high-power combiner has $20/400 \mu\text{m}$ core/cladding diameters. Therefore, a corresponding MFA is utilized for the reduction of signal light loss.

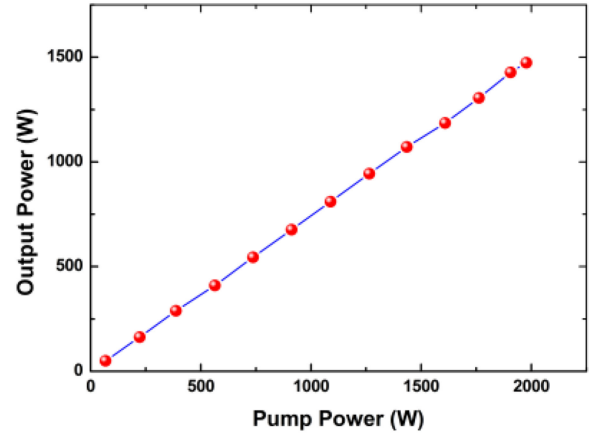


Fig. 9. Relationship between output and pump powers.

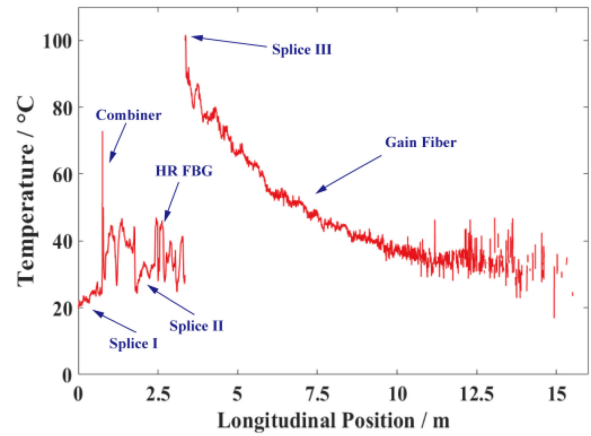


Fig. 10. Fiber-core temperature distribution in the fiber oscillator system with a 1.47 kW output power. Blue annotations indicate the temperature at different locations. Splice I: the splice between the MFA and combiner, HR FBG: high reflectivity FBG, Splice II: the splice between the combiner and HR-FBG, Splice III: the splice between the gain fiber and HR-FBG.

Before the experiment, we coiled the fiber on the heat sink without any nonnegligible residual strain. Then, an incubator was used to calibrate the fiber in the setup, which was introduced in section 2.2. The fiber laser system was based on antivibration optical platforms. The Rayleigh scattering signature was first measured as the reference profile in an ambient state before the measurement. In our experiment, the coiling diameter of the gain fiber was approximately 50 cm , and the cutting angle of the output fiber was 8° .

IV. RESULTS AND DISCUSSION

The dependence of the output power on the pump power is shown in Fig. 9. The output power of the laser oscillator increases almost linearly with the pump power, reaching 1474 W when the pump power is 1977 W . The efficiency of the laser oscillator is 74.6% . At an output power of 1.47 kW , the fiber-core temperature distribution was recorded by the measurement system, as shown in Fig. 10 with the red line. The blue annotations indicate the locations of different points and

components corresponding to Fig. 8. Many small fluctuations exist along the temperature distribution, which are caused by the system noise. Moreover, in approximately the last two meters along the gain fiber, many strong fluctuations, and even some data losses, can still be observed once the fiber laser breaks through the kilowatt-level output with our optimizations. The reason for this phenomenon is that the strength of the signal light becomes weaker after attenuations along the system to this last area. The signal light in this area is more easily affected by the main laser noise in the oscillator, which decreases the SNR and affects the results. Therefore, strong fluctuations can be observed when the fiber laser operates from low-level power to high-level power. Nevertheless, the above fluctuations have almost no effect on the trend analysis and study of the temperature distribution inside the fiber core.

From Fig. 10, we can find that the fiber core of the gain fiber is the highest temperature region in the entire fiber laser system. Due to forward pumping, the gain fiber shows a downward trend along the pumping direction. Moreover, Splice III, which is the splicing point between the HR-FBG and gain fiber, withstands the highest temperature, reaching 101.6 °C at a 1.47 kW output. This value of the real splicing-point temperature is much higher than the external temperature (~ 70 °C) that we can observe by a thermal imager. Except for at Splice III, the temperature of the gain fiber gradually decreases from the highest temperature point (92.0 °C) to approximately 30 °C along the pumping direction, which complies with the temperature distribution law of forward pumping.

Furthermore, the beam combiner and the HR-FBG are the two components that withstand the highest temperature apart from the gain fiber. Here, the fiber-core temperatures in the $(7 + 1) \times 1$ beam combiner and HR-FBG were measured. When withstanding a pump power of 1977 W, the internal temperature of the beam combiner reached 43 °C, while a temperature peak point of 73 °C appeared in front of the combiner. This temperature peak point will affect the performance of the beam combiner under high power conditions and become a limiting factor for higher power output. Meanwhile, the internal temperature of the HR-FBG reaches 45 °C, which is within the safe temperature range. The temperature of Splice I rises slightly because only the signal laser and backward laser propagate through it, rather than the main laser and pump laser. In addition, the fiber-core temperature at Splice II, which is between the combiner and HR-FBG, rises to only 33 °C, which reflects the good quality of the fusion splicing.

To verify the feasibility of the measurement experiment, we used the theoretical model introduced previously [21], [22] to simulate the fiber temperature of the kilowatt oscillator. In this model, rate equations for fiber lasers [36]–[39] and heat conduction equations for radial thermal distribution [12], [14] were combined. The parameters in the simulation are consistent with the experiment, which are shown in Table I. Here, for the heat sources, we took quantum defect heating and background loss in the fiber core into account.

Fig. 11 shows the comparison between the experimental results and the theoretical results, both with an output power of 1.47 kW. It is worth noting that the area our model simulates is

TABLE I
PARAMETERS IN THE MODEL

Symbol	Quantity	Value
λ_s	Wavelength of pump laser	976 nm
λ_p	Wavelength of main laser	1080 nm
a	Radius of fiber core	10 μm
b	Radius of inner cladding	200 μm
β	Cladding absorption at 976 nm	1.26 dB/m
H	Heat transfer coefficient	1200 $W / (cm^2 \cdot K)$
κ_f	Thermal conductivity in fiber	1.38 $W / (m \cdot K)$
α_s	Background loss for main laser	0.005 m^{-1}
α_p	Background loss for pump	0.003 m^{-1}
T	Ambient temperature	20 °C
L	Gain fiber length	12.5 m

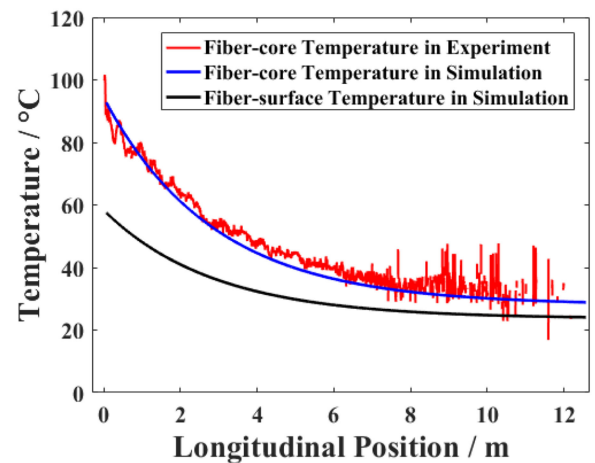


Fig. 11. Experimental and simulation results of the temperature in the gain fiber when the output power is 1.47 kW.

the temperature of the gain fiber except for at the splicing point. Therefore, the blue line and black line do not contain the temperature information of Splice III. From Fig. 11, the calculated temperature of the fiber core agrees well with our experimental measurement. Additionally, we can see a significant difference in the temperature between the fiber core and outside the fiber from the simulation results. The comparison not only shows the feasibility of the measurement system but also shows its superiority in the ability to measure the internal temperature of splicing points and the fiber core.

V. CONCLUSION

In this paper, based on the principle of OFDR and the feature of high-power fiber lasers, we analyzed the difficulties in applying OFDR to measure the fiber-core temperature in the high-power fiber laser regime. Methods for in situ measuring the fiber-core temperature in high-power fiber lasers were designed and optimized.

Based on the methods we proposed, the fiber-core temperature distribution in a kilowatt-level fiber laser oscillator was obtained. The temperature of the fiber core agreed well with our theoretical simulation. The methods realized fiber-core temperature distributed measurement from single-mode fibers to multimode fibers, from a low power level to a high power level, and from a laser amplifier to a laser oscillator. It is foreseeable that this method will provide strong support for our future study on thermal effects and thermal management in high-power fiber lasers.

REFERENCES

- [1] C. Jauregui, J. Limpert, and A. Tünnermann, "High-power fibre lasers," *Nat. Photon.*, vol. 7, pp. 861–867, Oct. 2013.
- [2] D. J. Richardson, J. Nilsson, and W. A. Clarkson, "High power fiber lasers: Current status and future perspectives," *J. Opt. Soc. Am. B*, vol. 27, no. 11, pp. B63–B92, 2010.
- [3] M. N. Zervas and C. A. Codemard, "High power fiber lasers: A review," *IEEE J. Sel. Top. Quantum Electron.*, vol. 20, no. 5, pp. 219–241, Sep/Oct. 2014.
- [4] B. Shiner, "The impact of fiber laser technology on the world wide material processing market," in *Proc. CLEO: Appl. Technol.*, 2013, Paper AF2J 1.
- [5] K. Shima, S. Ikoma, K. Uchiyama, Y. Takubo, M. Kashiwagi, and D. Tanaka, "5-kW single stage all-fiber Yb-doped single-mode fiber laser for materials processing," in *Proc. Fiber Lasers XV: Technol. Syst.*, San Francisco, CA, USA, vol. 10512, 2018, Paper 105120C, doi: [10.1117/12.2287624](https://doi.org/10.1117/12.2287624).
- [6] B. Yang *et al.*, "Monolithic fiber laser oscillator with record high power," *Laser Phys. Lett.*, vol. 15, no. 7, 2018. Art. no. 075106.
- [7] K. Sumimura, H. Yoshida, H. Okada, H. Fujita, and M. Nakatsuka, "Suppression of self pulsing in Yb-doped fiber lasers with cooling by liquid nitrogen," in *Proc. IEEE Conf. Lasers Electro-Opt.-Pacific Rim*, 2007, pp. 1–2.
- [8] W. Liu, J. Cao, and J. Chen, "Study on thermal-lens induced mode coupling in step-index large mode area fiber lasers," *Opt. Exp.*, vol. 27, no. 6, pp. 9164–9177, 2019.
- [9] M. N. Zervas, "Transverse mode instability, thermal lensing and power scaling in yb 3+ -doped high-power fiber amplifiers," *Opt. Exp.*, vol. 27, no. 13, 2019. Art. no. 19019.
- [10] R. Kashyap, "The fiber fuse - from a curious effect to a critical issue: A 25th year retrospective," *Opt. Exp.*, vol. 21, no. 5, pp. 6422–6441, 2013.
- [11] C. Jauregui, C. Stühler, and J. Limpert, "Transverse mode instability," *Adv. Opt. Photon.*, vol. 12, no. 2, pp. 429–484, 2020.
- [12] Y. Fan *et al.*, "Thermal effects in kilowatt all-fiber MOPA," *Opt. Exp.*, vol. 19, no. 16, pp. 15162–15172, 2011.
- [13] A. Mafi, "Temperature distribution inside a double-cladding optical fiber laser or amplifier," *J. Opt. Soc. Amer. B*, vol. 37, no. 6, pp. 1821–1828, 2020.
- [14] D. C. Brown and H. J. Hoffman, "Thermal, stress, and thermo-optic effects in high average power double-clad silica fiber lasers," *IEEE J. Sel. Top. Quantum Electron.*, vol. 37, no. 2, pp. 207–217, Feb. 2001.
- [15] M. Leich *et al.*, "Length distributed measurement of temperature effects in Yb-doped fibers during pumping," *Opt. Eng.*, vol. 53, no. 6, 2014, Art. no. 066101.
- [16] Q. Hu, P. Wang, M. Wang, and Z. J. Wang, "Fabrication of superimposed fiber bragg gratings and applications in fiber laser oscillators," *Optik*, vol. 214, 2020. Art. no. 164583.
- [17] F. Beier *et al.*, "In situ Temperature measurement in high power fiber amplifiers," in *Proc. Eur. Conf. Lasers Electro-Opt.*, 2015, Paper CJ_10_16.
- [18] F. Beier *et al.*, "Measuring thermal load in fiber amplifiers in the presence of transversal mode instabilities," *Opt. Lett.*, vol. 42, no. 21, pp. 4311–4314, 2017.
- [19] Z. Zhou, X. Wang, L. Huang, P. Ma, K. Han, and X. Xu, "Real time distributed temperature measurement of the gain fiber in all-fiber laser employing OFDR technology," *Appl. Opt. Photon. China*, 2017. Art. no. 10464.
- [20] B. Yang *et al.*, "3.05 kW monolithic fiber laser oscillator with simultaneous optimizations of stimulated raman scattering and transverse mode instability," *J. Opt.*, vol. 20, no. 2, 2018. Art. no. 025802.
- [21] Z. Lou, K. Han, X. Wang, H. Zhang, and X. Xu, "Increasing the SBS threshold by applying a flexible temperature modulation technique with temperature measurement of the fiber core," *Opt. Exp.*, vol. 28, no. 9, pp. 13323–13335, 2020.
- [22] L. Zhaokai *et al.*, "Real-time in-situ distributed fiber core temperature measurement in hundred-watt fiber laser oscillator pumped by 915/976 nm LD sources," *Sci. Rep.*, vol. 10, no. 1, 2020, Art. no. 9006, doi: [10.1038/s41598-020-66470-3](https://doi.org/10.1038/s41598-020-66470-3).
- [23] W. Eickhoff and R. Ulrich, "Optical frequency-domain reflectometry in single-mode fibers," *Appl. Phys. Lett.*, vol. 39, no. 9, pp. 693–695, 1981.
- [24] B. J. Sollerv, D. K. Gifford, M. S. Wolfe, M. E. Froggatt, M. H. Yu, and P. F. Wysocki, "Measurement of localized heating in fiber optic components with millimeter spatial resolution," in *Proc. Opt. Fiber Commun. Conf. Expo. Nat. Fiber Optic Eng. Conf.*, 2006, Paper OFN3.
- [25] B. J. Soller, D. K. Gifford, M. S. Wolfe, and M. E. Froggatt, "High resolution optical frequency domain reflectometry for characterization of components and assemblies," *Opt. Exp.*, vol. 13, no. 2, pp. 666–674, 2005.
- [26] M. E. Froggatt, D. K. Gifford, S. Kreger, M. Wolfe, and B. J. Soller, "Characterization of polarization-maintaining fiber using high-sensitivity optical-frequency-domain reflectometry," *J. Lightw. Technol.*, vol. 24, no. 11, pp. 4149–4154, 2006.
- [27] A. Güemes, A. Fernández-López, and B. Soller, "Optical fiber distributed sensing - Physical Principles and applications," *Struct. Health. Monit.*, vol. 9, no. 3, pp. 233–245, 2010.
- [28] D. K. Gifford *et al.*, "Swept-wavelength interferometric interrogation of fiber rayleigh scatter for distributed sensing applications," in *Proc. Fiber Optic Sensors Appl. V*, Boston, MA, USA, vol. 6770, 2007, Paper 67700F, doi: [10.1117/12.734931](https://doi.org/10.1117/12.734931).
- [29] D. K. Gifford, B. J. Soller, M. S. Wolfe, and M. E. Froggatt, "Distributed fiber-optic temperature sensing using rayleigh backscatter," in *Proc. 31st Eur. Conf. Opt. Commun.*, 2005, pp. 511–512.
- [30] S. T. Kreger, D. K. Gifford, M. E. Froggatt, B. J. Soller, and M. S. Wolfe, "High resolution distributed strain or temperature measurements in Single- and Multi-mode fiber using swept-wavelength interferometry," *Opt. Fiber Sensors*, 2006, Paper ThE42.
- [31] S. T. Kreger, A. K. Sang, D. K. Gifford, and M. E. Froggatt, "Distributed strain and temperature sensing in plastic optical fiber using rayleigh scatter," in *Proc. Fiber Opt. Sensors Appl. VI*, VI, Orlando, FL, USA, vol. 7316, 2009, Paper 73160A, doi: [10.1117/12.821353](https://doi.org/10.1117/12.821353).
- [32] Marcuse and D., "Field deformation and loss caused by curvature of optical fibers," *J. Opt. Soc. Amer.*, vol. 66, no. 4, pp. 311–320, 1976.
- [33] D. Marcuse, "Curvature loss formula for optical fibers," *J. Opt. Soc. Am.*, vol. 66, no. 3, pp. 216–220, 1976.
- [34] R. T. Schermer and J. H. Cole, "Improved bend loss formula verified for optical fiber by simulation and experiment," *IEEE J. Sel. Top. Quantum Electron.*, vol. 43, no. 10, pp. 899–909, Oct. 2007.
- [35] Y. Dongyong and G. E. Yubin, "Thermo-optic coefficient dependent temperature sensitivity of FBG-in-SMS based on sensor," *Ship Electron. Eng.*, vol. 39, no. 4, pp. 128–130, 2019.
- [36] I. Kelson and A. A. Hardy, "Strongly pumped fiber lasers," *IEEE J. Sel. Top. Quantum Electron.*, vol. 34, no. 9, pp. 1570–1577, Sep. 1998.
- [37] I. Kelson and A. Hardy, "Optimization of strongly pumped fiber lasers," *J. Lightw. Technol.*, vol. 17, no. 5, pp. 891–897, 1999.
- [38] H. Yu, X. Wang, R. Tao, P. Zhou, and J. Chen, "1.5 kW, near-diffraction-limited, high-efficiency, single-end-pumped all-fiber-integrated laser oscillator," *Appl. Opt.*, vol. 53, no. 34, 2014. Art. no. 8055.
- [39] M. Gong, Y. Yuan, C. Li, P. Yan, H. Zhang, and S. Liao, "Numerical modeling of transverse mode competition in strongly pumped multimode fiber lasers and amplifiers," *Opt. Exp.*, vol. 15, no. 6, pp. 3236–3246, 2007.

Zhaokai Lou received the B.S. and M.S. degrees in optical engineering, in 2015 and 2017, respectively, from the National University of Defense Technology, Changsha, China, where he is currently working toward the Ph.D. degree with the College of Advanced Interdisciplinary Studies. His research focuses on the temperature characteristics of high-power fiber laser systems.

Kai Han received the B.S. and Ph.D. degrees in optical engineering from the National University of Defense Technology, Changsha, China, in 2008 and 2013, respectively. He is currently an Associate Professor with the College of Advanced Interdisciplinary Studies, National University of Defense Technology. His current research interests include fiber laser or amplifier technology and laser-induced damage in high-power laser systems.

Baolai Yang received the B.S. degree in optical engineering from the University of Electronic Science and Technology of China, Chengdu, China, in 2012 and the Ph.D. degree in optical engineering from the National University of Defense Technology, Changsha, China, in 2019. He is currently a Lecturer with the College of Advanced Interdisciplinary Studies, National University of Defense Technology. His current research focuses on high-power fiber lasers.

Hanwei Zhang received the B.S. and Ph.D. degrees in optical engineering from the National University of Defense Technology, Changsha, China, in 2010 and 2015, respectively. He is currently a lecturer with the College of Advanced Interdisciplinary Studies, National University of Defense Technology. His current research interests include random fiber lasers and high-power fiber lasers.

Xiaoming Xi received the B.S. degree in optical engineering from the University of Electronic Science and Technology of China, Chengdu, China, in 2008 and the Ph.D. degree from the Max Planck Institute, in 2015. He is currently a Lecturer with the College of Advanced Interdisciplinary Studies, National University of Defense Technology. His current research focuses on high-power fiber lasers.

Xiaolin Wang received the B.S. degree in optical engineering from the University of Electronic Science and Technology of China, Chengdu, China, in 2006 and the Ph.D. degree in optical engineering from the National University of Defense Technology, Changsha, China, in 2011. He is currently an Associate Professor with the College of Advanced Interdisciplinary Studies, National University of Defense Technology. His current research focuses on high-power fiber lasers.

Xiaojun Xu received the B.S. and Ph.D. degrees in optical engineering from the National University of Defense Technology, Changsha, China, in 1995 and 2000, respectively. He is currently a Professor with the College of Advanced Interdisciplinary Studies, National University of Defense Technology. His current research interests include high-power fiber lasers and adaptive optics.

Zejin Liu received the B.S. degree from Shandong University, Jinan, China, in 1983 and the Ph.D. degree in optical engineering from the National University of Defense Technology, Changsha, China, in 1997. He is currently a Professor and Academician with the College of Advanced Interdisciplinary Studies, National University of Defense Technology. His current research interests include fiber laser or amplifier technology, high-power lasers, and laser-induced damage in high-power laser systems.